Int. J. Electrochem. Sci., 8 **(2013)** 11596 - 11605

International Journal of
ELECTROCHEMICAL
SCIENCE
www.electrochemsci.org

Upright-Standing SnO_2 Nanosheets Glazed CdSe Nanocrystallites: High Photocurrent Generating Photoelectrochemical Cells

Sambhaji S. Bhande[1,2], *Eun-kyung Kim*[2], *Dipak V.Shinde*[2], *Supriya Patil*[2], *Rajaram S. Mane*[1,2,*], *Sung-Hwan Han*[2,*]

[1] Center for Nanomaterials and Energy Devices, School of Physical Sciences, SRTM University, Nanded, India-431606, Email: rsmane_2000@yahoo.com
[2] Inorganic Nanomaterials Laboratory, Department of Chemistry, Hanyang University, Seoul 133-791, Seoul, Korea. FAX:+82-2-2299-0762;Tel no:+82-2-2220-0934;
[*]E-mail: shhan@hanyang.ac.kr, rsmane_2000@yahoo.com

Received: 29 March 2013 / *Accepted:* 2 August 2013 / *Published:* 20 August 2013

Efficient charge separation in photoelectrochemical cell composed of solution-processed SnO_2 nanosheets (NSs)-CdSe nanocrystallites (NCs), is investigated. The SnO_2 NSs decorated with CdSe NCs, confirmed from the structural elucidation and morphological evolution studies, electrode exhibited 16.40 mA/cm^2 and 2.70% short circuit current density and power conversion efficiency which were superior to pristine CdSe nanowires-based electrode (9.44 mA/cm^2, 1.44%). This increment was caused by relatively smaller recombination losses followed by higher electron life time and was well-supported from the photoluminescence, incident photon-to-current efficiency and electrochemical impedance spectroscopy measurements.

Keywords: Photo electrochemical cells; Photoluminescence; impedance spectroscopy.

1. INTRODUCTION

Pollution-free conversion of solar energy into electricity using solution-proceed solar cells is cost-effective to manufacture and offer the potential of physical flexibility.[1] Recent inventions in solar cells are extensively focused on the use of semiconducting nanocrystals (NCs) due to various outstanding features associated with them.[2] The versatile (size and shape dependent) optoelectronic properties of NCs are being considered as the main focus in ongoing research activities.[3,4] High molar extinction coefficient, broad absorption for covering visible region of the solar spectrum [5] and multiple exciton generation ability [6] etc., of NCs are incredible. Several NCs including CdSe, CdS, PbS and PbSe etc., have been envisaged as light absorbing materials in several studies[7-10]. Using a

passivating layer, carbon nanotubes, modified electrolytes and counter electrode (other than platinum) efficient charge transportation and separation with less recombination losses, with several orders of magnitudes enhanced power conversion efficiency, were achieved as on today.[11-15] Photoelectrochemical (PEC) cells of semiconducting NCs show relatively inferior performance due to serious recombination losses on account of; a) the electron transport route referred as random walk, and b) lack of electrolyte at interior portion which cannot reach to the inner part, in particular, when relatively thick NCs layer is employed.[16] Using variety of metal oxides as such TiO_2, SnO_2, ZnO etc., as templates, and covering them with a metal chalcogenide NPs monolayers (CdS, CdSe, PbS etc.) these limitations are partially suppressed and a higher power conversion efficiency can be achieved.[17]

It is mandatory that the conduction band level of preferred metal oxide should be at lower position than NCs and must have higher carrier charge mobility. Tin oxide (SnO_2), amongst available large band gap metal oxides, would be a better choice [18] as it has higher electron mobility (240 $cm^2/(Vs)$) and electronic conductivity as compare to TiO_2 and ZnO. More negative conduction band minimum (~0.40 eV, compared to anatase TiO_2) suggests effective charge separation and transportation from the photosensitizer. One-dimensional metal oxide architectures such as wire, pine-tree, hierarchical, rods, etc., reveal better charge collection efficiency. The NCs of high surface area facilitate the more light harvesting efficiency than other architectures. Charge carriers, with minimum recombination losses, are separated across the metal oxides interfaces of appropriate positions. Therefore, by employing variety of metal oxide architectures and covering them with semiconducting NCs, efficient charge separation, with minimum recombination losses, followed by higher power conversion efficiency can be achieved.

In continuation to our ongoing research activities,[19] in this communication, we report SnO_2 nanosheets (NSs)-glazed CdSe NCs PEC cell with 16.40 mA/cm^2 short-circuit current density (J_{sc}) which is substantially higher than SnO_2 NSs-free CdSe electrode (9.66 mA/cm^2). This enhancement is corroborated by a favorable positive photoluminescence (PL) quenching effect. An enhanced incident photon-to-current emission (IPCE) and decreased charge transfer resistance are responsible for higher exciton separation, in presence of SnO_2, than pristine CdSe electrode.

2. EXPERIMENTAL DETAILS

The arrays of SnO_2 NSs were hydrothermally grown using wet-chemistry at 70 ^oC. For growing SnO_2 NSs, tin chloride and thioacetamide chemical precursors were dissolved in ethanol solution in 1:2 ratio. The reaction was terminated after 2 h. The details about chemical kinetics and the NSs formation mechanism are obtained from our recent work [20]. For glazing SnO_2 NSs with CdSe NCs, electrodeposition method was preferred. [21] in brief, synthesis is carried out as follows;

2.1. Synthesis of SnO_2 nanosheets

All the chemicals were purchased from Sigma-Aldrich and used without further purification. For the synthesis of SnO_2 nanosheets, initially 0.2 M tin tetrachloride ($SnCl_4$) was taken in ethanol

solvent for 50 ml, after dissolving it, 0.4 M thioacetamide was further added to the same solution. The solution was then sealed in a falcon tubes of 50 ml with two FTO substrates of 8 × 2.5 cm inserted and kept vertically into it facing in opposite direction to each other. Prior to the FTO substrates used for deposition were firstly cleaned with detergent solution, then with isopropanol and acetone solution by ultrasonication for 30 minutes, dried in an argon gas flow and then treated in ozone for 15 minutes. The chemical bath deposition was carried out at 70 ºC, the reaction was terminated in order to control the thickness of the film after 2 h. The films thus obtained were washed with ethanol and naturally dried in air and then annealed at 450 ºC for 1 hr. thus, the film obtained by this method is of one micron thickness and is transparent in nature with uniform coverage over the surface.

2.2. Electrodeposition of CdSe

Electrodeposition of CdSe was carried out at room temperature. Initially an aqueous solution of 0.05 M of cadmium sulphate which acts as a source of metallic ions and 0.01 M selenium oxide releasing cationic ions in the prepared electrolyte solution for deposition. The electrodeposition was carried in three electrode system for 30 minutes, in order to control the monolayer coverage of the CdSe nanoparticles over SnO_2 nanosheets. The surface area of 1× 1 cm^2 was taken for the electrodeposition process with bare FTO and SnO_2 nanosheets covered FTO as working electrode. A constant current density of 2 mA is applied in presence of Platinum plate as counter electrode and Ag/AgCl as reference electrode. For the uniform coverage of the film the distance between working and counter electrode was kept small (~ 0.5 cm) with parallel arrangement to each other. The obtained films were black in color and shining in appearance.

These as synthesized films were then annealed at 300 ºC for 1 h for crystallinity improvement and used for further characterizations.

2.3 Characterization techniques

Crystal structure of the as synthesized electrodes was determined using X-ray diffractometer (XRD) (Rigaku D/MAX 2500 V, Cu Kα, λ = 1.5418 ºA). The thickness and morphology of the samples prepared were analyzed with a scanning electron microscope (SEM, Hitachi S-4200). The UV-Visible analysis was carried out by using a carry 100 UV-Visible spectrophotometer. To measure the diffused absorbance, initially the % reflectance spectrum was taken which was then converted to absorbance using the same software of Carry winUV. A Hololab series 5000 Raman spectroscopy (Kaiser Optical System, Inc.) is used for raman analysis. Solar-to-electric power conversion efficiency of the devices were measured by, incorporating individual cell with an active area of 0.5 cm×0.5 cm was sealed using a spacer film (50 μm thick polyester film) with polysulphide electrolyte composed of 0.5 M Na_2S, 2 M S and 0.2 M KCl (for enhancing electrolyte conductivity) in a methanol/water (7:3 by volume). A Pt-coated FTO was used as counter electrode which was prepared by a drop casting method. For the preparation of counter electrode, 0.04 M isopropanol solution of chloroplatinic acid was drop casted on FTO followed by heating at 450 deg for 20 minute. Cell performance was

measured by irradiation with 100 mW/cm^2 white light (1 Sun) with a solar simulator in the presence of a water filter (450 W xenon lamp, Oriel Instruments). Current were measured by using a Keithley 2400 source meter. Electrochemical impedance spectrum (EIS) were recorded with an Impedance Analyzer (COMPACTSTATe: IVIUM Technologies) in a frequency range of 0.01 Hz to 1.5 MHz with 50 mV amplitude. The measurements of EIS were carried out at open circuit potentials under 1 sun AM 1.5 G light illumination. Impedance parameters were determined by fitting impedance spectra using Z-view software.

3. RESULT AND DISCUSSION

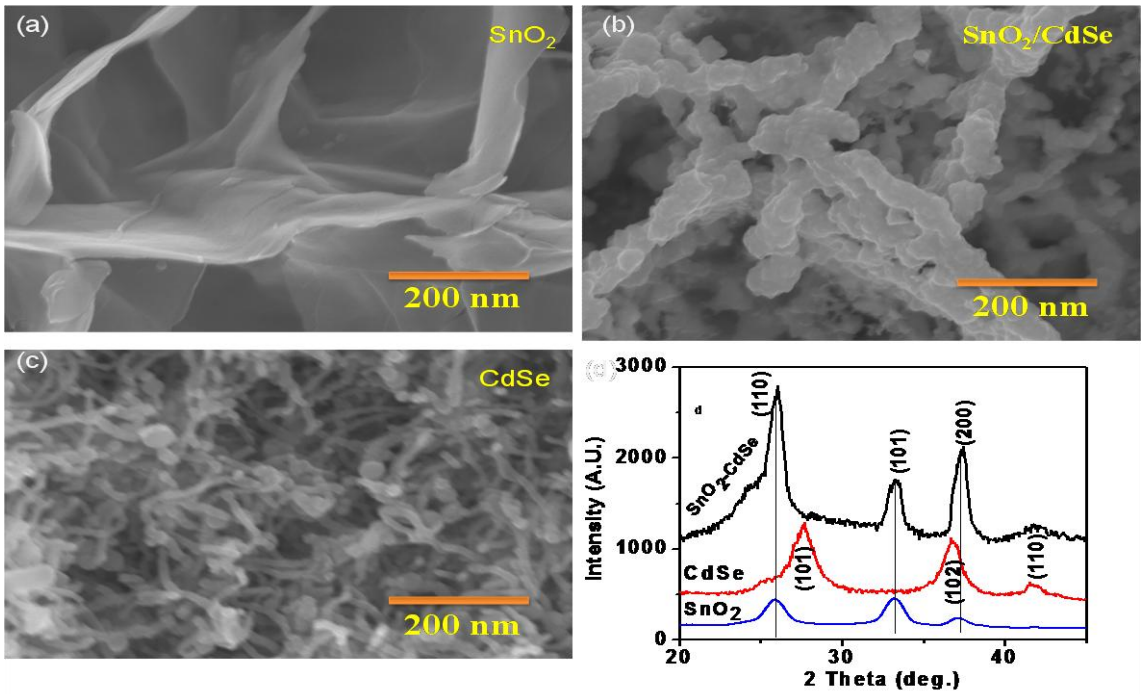

Figure 1. FE-SEM images of; (a) SnO_2 NSs, (b) SnO_2 NSs-CdSe NCs, (c) CdSe NWs, and (d) corresponding X-ray diffraction spectra.

Fig. 1 presents the FE-SEM images of steriospecifically grown SnO_2 NSs, CdSe NCs glazed SnO_2 NSs, SnO_2 NSs free electrodeposited CdSe (nanowires, NWs) electrodes and their respective XRD measurements. Ultrathin SnO_2 NSs of 20-30 nm in widths [Fig. 1 (a)] were grown perpendicular to substrate surface measured. These NSs were well-separated from each other with voids of irregular dimensions. Right after electrodepositing process these thin SnO_2 NSs were well-decorated with NCs of CdSe. It was difficult to trace-out an individual SnO_2 sheet after glazing CdSe NCs [Fig. 1 (b)]. Interestingly, without SnO_2 NSs presence the growth form of CdSe was completely different [Fig. 1 (c)]. These NWs were few micrometers in lengths and 40-60 nm in diameters, similar to our previous observations.[20] It is noted that while forming the CdSe NCs instead of NWs involvement of base SnO_2 NSs layer has prime importance. Here, SnO_2 NSs, first form, act nucleation centres for growing CdSe NCs as a secondary form. The X-ray diffraction spectra of SnO_2 NSs, CdSe NWs and SnO_2 NSsglazed CdSe NCs electrodes are plotted in Fig. 1 (d). Rutile tetragonal and wurtzite structures,

respectively, were confirmed for SnO_2 NSs and CdSe NWs (JCPDS: SnO_2-41-1445; CdSe-08-0459). The (101), (102) and (110) reflection planes were seen in XRD plot of CdSe NWs. Due to change in form from wire to sphere, the (101) and (102) planes of CdSe were completely diminished, suggesting that during CdSe growth, as secondary phase, over primary i.e. SnO_2 *c*-axis coverage is restricted.

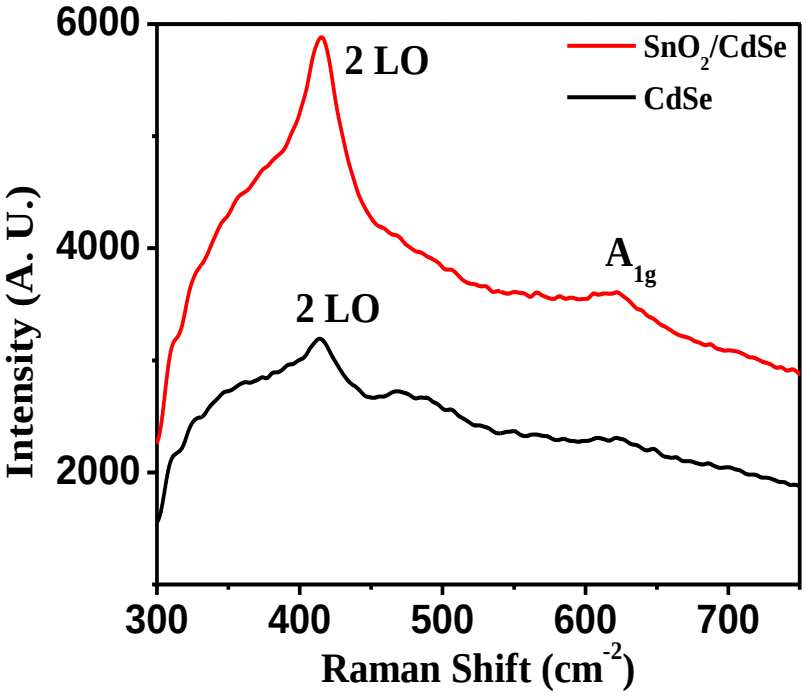

Figure 2. Raman analysis of SnO2/CdSe and CdSe films

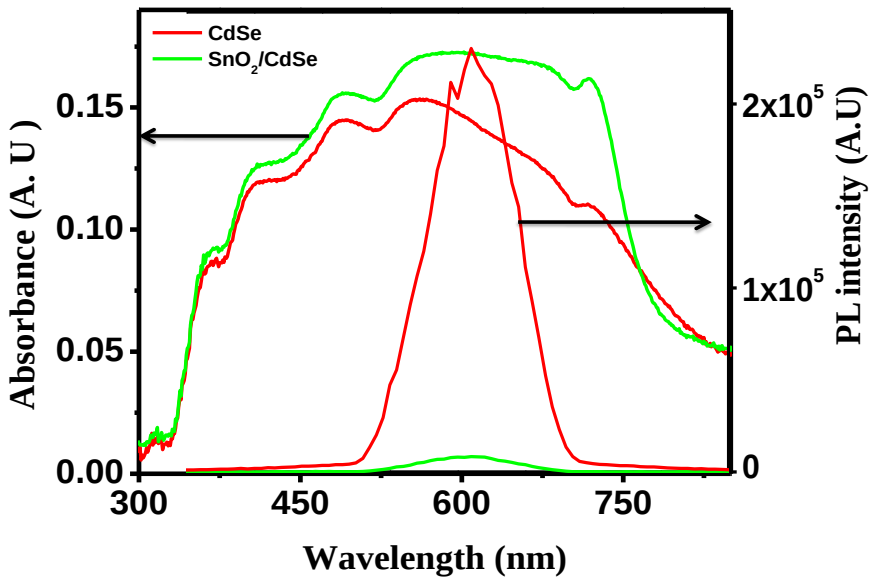

Figure 3. Diffused UV-Visible and the Photoluminescence spectra of CdSe NWs and SnO_2 NSs-CdSe NWs electrodes.

The CdSe NCs formation over SnO_2 NSs was evidenced from the Raman measurement (Fig. 2). The Raman spectrum of the samples were collected with a Horiba–Jobin Yvon LabRam-HR spectrometer equipped with a confocal microscope, 2400/900 grooves mm^{-1} gratings, and a notch filter. The visible laser excitation at 532 nm (visible/green) was used. The scattered photons were directed and focused onto a single-stage monochromator and measured with a UV-sensitive LN2-cooled CCD detector. The raman spectrum shows a peak at 414.75 cm^{-1} wavenumber which corresponds to 2LO energy level of CdSe, which becomes more intense in the case of SnO_2/CdSe electrode analysed at the same time the A_{1g} peak is observed corresponding to SnO_2. In addition to SnO_2 A_{1g} peak at 621 cm^{-1}, [20] CdSe peak at 416 $cm^{-1,}$ [22] was due to 2LO energy level of CdSe in SnO_2 NSs glazed CdSe NCs electrode. The diffused absorbance and PL measurements, recorded at room temperature, for CdSe NWs and SnO_2 NSs-CdSe NCs electrodes are shown in Fig. 3. The strong absorbance within 350-770 nm was noticed for both electrodes. Sharp adsorption edge, for both electrodes, at 770 nm was attributed to bulk CdSe band gap (~1.7 eV). Optical density of SnO_2 NSs-CdSe NCs electrode was slightly higher than CdSe NWs electrode. Effective charge separation and fast charge transportation in SnO_2 NSs glazed CdSe NCs electrode, than CdSe NW electrode, were corroborated from the PL and the EIS measurements. The SnO_2 NSs glazed CdSe NCs electrode showed a perfect positive quenching effect [23] over CdSe NWs electrode suggesting that SnO_2 NSs-CdSe NCs interface is more favourable for charge separation followed by transportation with minimum recombination losses. Lower conduction band position and higher electron mobility of SnO_2 over CdSe would be responsible to improve the electron transfer and transport characteristics. [24, 25]

Fig. 4(a) identifies the *J-V* measurements of CdSe NWs and SnO_2 NSs-CdSe NCs electrodes tested with an area of 0.25 cm^2 under 100 mW/cm^2 light intensity. The CdSe NWs electrode showed 9.66 mA/cm^2 current density (J_{sc}) and 1.44% power conversion efficiency whereas, SnO_2 NSs glazed CdSe NCs electrode confirmed nearly double J_{sc} i.e. 16.40 mA/cm^2 and a power conversation efficiency of 2.70% with a negligible variation in an open circuit voltage and fill factor values. The J_{sc} value obtained in this work is superior to reported elsewhere [26] and close to SnO_2-CdS/CdSe electrode (i.e. 17.40 mA/cm^2) [27]. Increase in current density of 55% in presence of SnO_2 NSS is due to efficient charge separation/transfer process. Band position different between the SnO_2 and the CdSe is prohibiting injected electrons to follow reserve path. Secondly, direct pathway in SnO_2 NSs, free from the random percolation of photoinjected electrons, is advantageous for the least charge transfer resistance followed by prolonged electron life time. Fig 4(b) confirms the IPCE measurements for CdSe NWs and SnO_2 NSs glazed CdSe NCs electrodes. An increment in external quantum efficiency by 55%, is a reason for boost in photocurrent density as seen in *J-V,* due to electron separation/transfer from CdSe NCs to SnO_2 NSs was achieved.

To have an in-depth PEC performance understanding EIS measurement was operated on both electrodes. Details about Nyquist plots and an equivalent circuit (with fitting parameters) are presented in figure 5, for CdSe and SnO_2/CdSe photo-electrode tested for QDSSCs. The inset shows an equivalent circuit used for the analysis. The second arc in the figure above indicates the recombination resistance of the photogenerated electron. Moreover the reduction in frequency of the peak value of second arc which is inversely proportional to the electron lifetime, confirms nearly doubling of electron life time. The various parameters of QDSSCs and EIS obtained are summarized in Table 1.

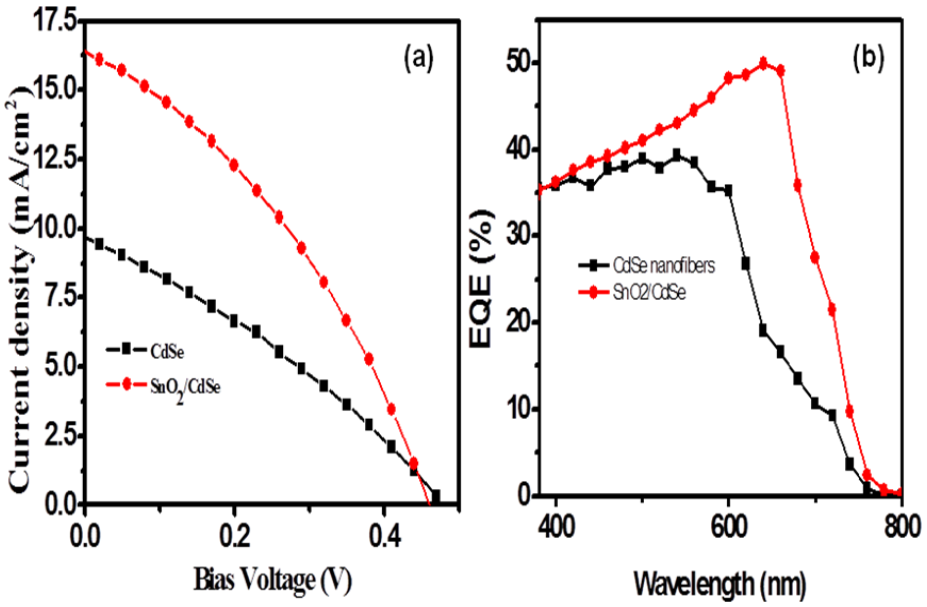

Figure 4. (a) Current density-voltage and, (b) IPCE measurements of CdSe NWs and SnO_2 NSs-CdSe NWs electrodes.

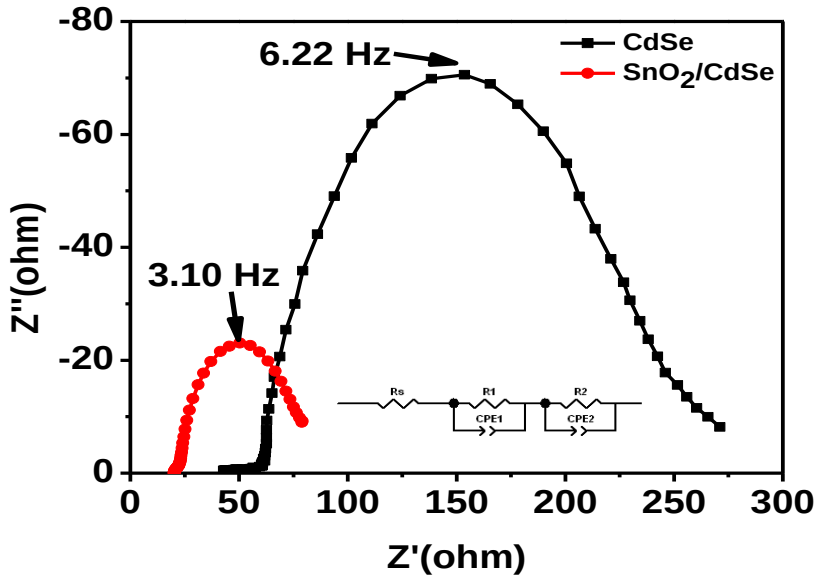

Figure 5. Electrochemical impedance spectra of CdSe and SnO_2/CdSe photoelectrode fabricated.

The CPE symbol was assigned to the constant phase element of the capacitance. The elements with subscripts 1 and 2 were related to the capacitance of the interfaces of the electrolyte/platinum counter electrode and photoelectrode/electrolyte, respectively. Smaller second semicircle for SnO_2 NSs-CdSe NCs electrode than for CdSe NWs electrode was an indication for fewer recombination losses. The cascade system formed between the SnO_2 NSs and CdSe NCs, with favourable alignment of the conductions bands, facilities efficient charge separation/transportation across the interface. A

uniform and total surface coverage of SnO_2 NSs with CdSe NCs can block the electrolyte-SnO_2 interaction and prohibit the possibility of electron recombination with electrolyte. The peak frequencies of 6.22 and 3.10 Hz were recorded for CdSe NWs and SnO_2 NSs-CdSe NCs electrodes, respectively, from which the electron life times were estimated. Electron life times for CdSe NWs and SnO_2 NSs-NCs electrodes were 25.58 and 51.33 ms, respectively. An improvement in life time of 200% was due to substantial retardation in the interfacial recombination losses for NSs-NCs interfaces than CdSe NWs. The prolonged electron life time in SnO_2 NSs-CdSe NCs electrode than CdSe NWs electrode, negligible charge carriers for recombination with S^{2-} ions in the electrolyte [28], was responsible for improving charge separation and as a consequence, better photocurrent generation.

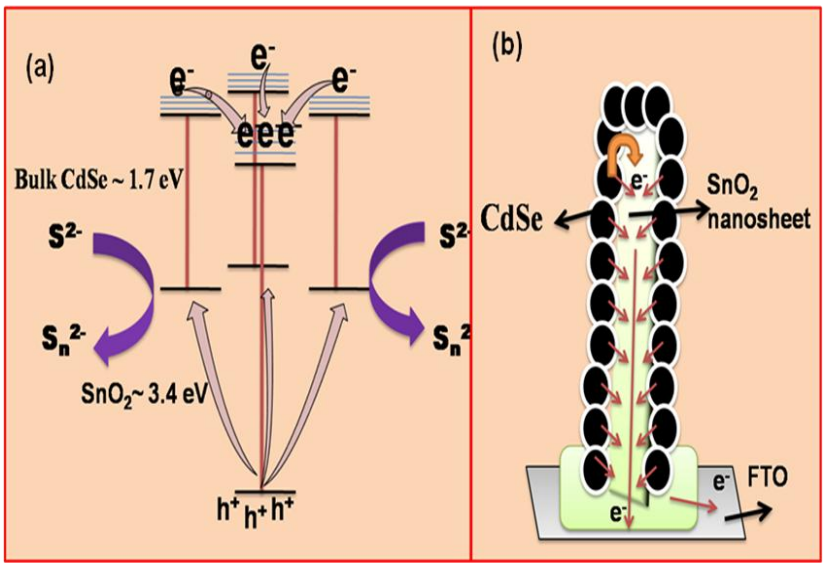

Figure 6. (a) Energy band diagram for electron transport route and, (b) a cartoon image of SnO_2 NS covered with several CdSe NCs.

Fig. 6 (a) depicts a schematic representation of electronic states of assembly undertaken with respective band position levels. We presumed that increase in photocurrent was due to the generation of favourable Fermi band level alignment as CdSe NCs were grown onto the SnO_2 NSs otherwise there could be a straddling band structure when grown directly on the transparent electrode. [29, 30]

Fig. 6(b) provides a cartoon image showing the photoelectrons transfer track from CdSe NCs to SnO_2 NSs. Due to a linker-free direct attachment of uniformly decorated CdSe NCs the photogenerated electrons can inject into the upright-standing SnO_2 NSs matrix and then there is a direct transportation to charge collecting electrode. This may produce higher photocurrent than assembly wherein several percolation steps are involved.

4. CONCLUSION

In nutshell, CdSe electrode showed 70% increase in photocurrent due to 55% increase in IPCE caused by 200% increase in electron life time. This facilitates a positive quenching effect and least

charge transfer resistance in SnO_2-CdSe electrode compared with pristine CdSe electrode. Presence of CdSe NCs over SnO_2 NSs was confirmed form the XRD and Raman measurements. Without SnO_2, form of CdSe was different indicating that layer of NSs, primary, plays a vital role during CdSe, secondary, growth process. This strategy can also be applied in several metal oxides/CdSe interfaces for enhancing the photocurrent followed by conversion efficiency, which is ongoing topic of research.

ACKNOWLEDGMENT
This work was supported by the "KIST institutional program" (2E23964) and Technology Innovation Program (K00060-602) funded by the Ministry of Knowledge Economy.

References

1. M. Graetzel, R. A. Janseen, D. B. Mitzi and E. H. Sargent, *Nature*, 488 **(**2012) 304.
2. Z. Yang, C. Y. Chen, P.Roy and H. T. Chang, *Chem. Commun.*, 47 (2011) 9561.
3. A. M. Smith and S. M. Nie, *Acc. Chem. Res.*, 43 (2010) 190.
4. A.Kongkanand, K. Tvrdy, K.Takechi, M. Kuno, and P. V. Kamat, *J. Am. Chem. Soc.*, 130 (2008) 4007.
5. L. Etgar, J. Park , J. Barolo, V. Lesnyak , S. K. Panda, P. Quagliotto, S. G. Hickey, Md. K. Nazeeruddin, A. Eychmuller, G. Viscardi and M. Gratzel, *RSC Advances*, 2 (2012) 2748.
6. W. A. Tisdale, K. J. Williams, B. A. Timp, D. J. Norris, E. S. Aydil and X. Y. Zhu, *Science*, 328 (2010) 1543.
7. L. M. Peter, D. J. Riley, E. J. Tull and K. G. U. Wijayantha, *Chem. Comm*., 10 (2002) 1030.
8. R. J. Ellingson, M. C. Beard, J. C. Johnson, P. Yu, O. I. Micic, A. J. Nozik, A. Shabaev and A. L. Efros, *Nano Lett.*, 5 (2005) 865.
9. R. Debnath,; J. Tang, D. A.Barkhouse, X. Wang, A. G. Pattantyus-Abraham, L. Brzozowski, L. Levina and E. H. Sargent, *J. Am. Chem. Soc.*, 132 (2010) 5952.
10. R. D. Schaller and V. I. Klimov, *Phys. Rev. Lett.* 92 (2004) 186601.
11. P. K. Santra and P. V. Kamat, *J. Am. Chem. Soc.*, 134 (2012) 2508.
12. G. Y. Lan, Z. S. Yang, Y. W. Lin, Z. H. Lin, H. Y. Liao and H. T. Chang, *J. Mater. Chem.*, 19 (2009) 2349.
13. H. J. Lee, J. H. Yum, H. C. Leventis, S. M. Zakeeruddin, S. A. Haque, P. Chen, S. I. Seok, M. Gratzel, and M. K. Nazeeruddin, *J. Phys.Chem. C*, 112 (2008) 11600.
14. B. Fang, M. Kim, S. Q. Fan, J. H. Kim, D. P. Wilkinson, J. Ko and J. S. Yu, *J. Mater. Chem.*, 21 (2011) 8742.
15. M. Wu and T. Ma, *Chem. Sus. Chem.*, 5 (2012) 1343.
16. I. V. Lightcap and P. V. Kamat, *J. Am. Chem. Soc.* 134 (2012) 7109.
17. E. Hendry, M. Koeberg, B. O'Regan and M. Bonn, *Nano Lett.;* 6 (2006) 755.
18. R. E. Chandler, A. J. Houtepen, J. Nelson, D. Vanmaekelbergh, *Phys. Rev. B*, 75 (2007) 085325.
19. R. S. Mane, D. V. Shinde, S. J. Yoon, Ambade, S. B.; Lee, J. K.; Han, S. H. *Appl. Phys. Lett.,* 101 (2012) 33906.
20. D. V. Shinde, R. S. Mane, I. H. Oh, J. K. Lee and S. H. Han, *Dalton Trans*., 41 (2012) 10161.
21. S-K. Min, O-S Joo, K-D. Jung, R. S. Mane and S-H. Han, *Electrochem. Commun.*, 8 (2006) 223.
22. T. Ganesh, J. H. Kim, S. J. Yoon, S. Lee, W. J. Lee, R. S. Mane, J. W. Han and S-H. Han, *J. Appl. Phys.*, 106 (2009) 84304.
23. M. G. Syed Basheer Ahamed, A. R. Balu, V. S. Nagarethinam, A. Thayumanavan, K. R. Murali, C. Sanjeeviraja, M. Jayachandran, *Cryst. Research Tech.*, 45 (2010) 387.

24. E. M. Barea, M. Shalom, S. Gimeenez, I. Hod, I. Mora-Sero, A. Zaban, J.Bisquert; *J. Am. Chem. Soc.*, 132 (2010) 6834.
25. I. Robel, V. Subramanian, M. Kuno, P. V. Kamat, *J. Am. Chem. Soc.*, 128 (2006) 2385.
26. G. Zhu, L. Pan, T. Xu, Z. Sun, *ACS Appl. Mater. Interfaces*, 3 (2011) 3146.
27. M. Gratzel, *Nature*, 414 (2001) 338.
28. M. A. Hossain, J. R. Jenning, Z. Y. Koh, Q. Wang, *ACS Nano*, 5 (2011) 3172.
29. Y. L. Lee, Y. S. Lo, *Adv. Funct. Mater.*, 19 (2009) 604.
30. Y. Tak, S. J. Hong, J. S. Lee, K. Yong, *Crystal Growth Design*. 9 (2009) 2627.